Environmental Science and Pollution Research (2022) 29:17280–17294
https://doi.org/10.1007/s11356-021-16971-z

RESEARCH ARTICLE

New models for calculating the electrical resistivity of loess affected by moisture content and NaCl concentration

Zhao Duan[1,2] · Xusheng Yan[1,2] · Qiang Sun[1,2] · Xuan Tan[1,2] · Xin Chen[3,4,5]

Received: 12 July 2021 / Accepted: 6 October 2021 / Published online: 18 October 2021

Abstract

Saline loess is an important cause of environmental geo-issues in northwest China. In this research, electrical resistivity of loess with different moisture contents and NaCl concentrations was measured at three test frequencies. Results indicates the plastic limit (16%) and around 2% NaCl concentration are the critical content affecting the variation of loess electrical resistivity. The variation and conductivity for conductive paths are affected by moisture content and NaCl concentration respectively. Combined with three-phase composition and diffuse double-layer structure, new models that consider the effect of moisture content and NaCl concentration indicate good applicability in the validation datasets from different types of soil. A new model was verified by comparison between previous studies and experimental results. This research provides (i) theoretical support for the calibration of large-scale electrical field surveys and the observation of saline loess and (ii) a valuable reference for the prevention of environmental geo-crisis and the utilization of soil resources in northwestern China.

Keywords Loess · Electrical resistivity · Three-phase structure · Conductive path · Diffuse double layer · Theoretical model

Introduction

Loess is associated with various environmental geohazards that threaten people and infrastructure in the widespread loess region of northwestern China (Chang et al. 2021a, 2021b; Duan et al. 2021b, 2020; Yin et al. 2021), so it is necessary to investigate the loess properties in this area. The perennial arid environment of northwestern China means that agriculture requires large-area irrigation, which affects groundwater levels and causes serious soil salinization (Weisbrod and Dragila 2006). Previous studies have found that salinity has significant influences on environmental geo-crisis such as landslides, debris flows, and ground collapses (Fan et al. 2017; Fu et al. 2019; Li et al. 2020a; Wang et al. 2019). Therefore, it is urgent to investigate the properties of loess under the influence of water and salt.

In recent years, field surveys using electrical resistance technology (ERT) have been widely used in the investigation of geo-materials, and play an important role in field monitoring and assessment of water infiltration in soil (De Jong et al. 2020; Sendrós et al. 2020; Zhao et al. 2020), groundwater potential assessments (Doetsch et al. 2012; Hasan et al. 2019; Joel et al. 2019), soil liquefaction (Ronald and Ronald 1982), and the stability evaluation of geo-materials (Kemna et al. 2002; Park et al. 2017; Snapp et al. 2017; Zhou and

Responsible Editor: Philippe Garrigues

✉ Xusheng Yan

✉ Qiang Sun
sunqiang04@cumt.edu.cn

Zhao Duan
duanzhao@xust.edu.cn

Xuan Tan
tx199511@163.com

Xin Chen
chenxin182@mails.ucas.edu.cn

[1] College of Geology and Environment, Xi'an University of Science and Technology, Xi'an 710054, China

[2] Shaanxi Provincial Key Laboratory of Geological Support for Coal Green Exploitation, Xi'an 710054, China

[3] State Key Laboratory of Geomechanics and Geotechnical Engineering, Institute of Rock and Soil Mechanics, Chinese Academy of Sciences, Wuhan 430071, China

[4] University of Chinese Academy of Sciences, Beijing 100049, China

[5] IRSM-CAS/HK PolyU Joint Laboratory On Solid Waste Science, Wuhan 430071, China

Che 2020; Zhou et al. 2002). As a non-invasive method, ERT avoids significant damage to geotechnical materials and has the advantages of wide detection range and simple operation (Tabbagh et al. 2007). However, ERT is often limited by the complex topography and poor working environments of field sites, which can cause inaccurate results (Hen Jones et al. 2014). Meanwhile, the electrical resistivity theory of the Archie model originated from pure sandstone has been extended to a variety of other geo-materials (Cai et al. 2017; Ellis et al. 2010; Rhoades and Schilfgaarde 1976). Combined with laboratorial experimental methods, some researchers revealed the electrical resistivity of geotechnical materials from a new perspective (Erzin et al. 2010; Ozcep et al. 2010; Yin et al. 2021). Laboratory electrical resistivity tests have been widely used in the study of silty clay (Rinaldi Victor and Cuestas German 2002), marine clay (Zhang et al. 2014), expansive soil (Chu et al. 2018), compacted kaolin (Cardoso and Dias 2017), and loess (Liu et al. 2014; Zha et al. 2010) for their rapid, economical, and easy-to-use techniques, and accurate test results (Samouëlian et al. 2005). Therefore, it is a feasible method to obtain the characteristic parameters and their variation law of geotechnical materials through laboratory test method (Tang et al. 2018; Zhou et al. 2015), which can provide reference for field geophysical test and reduce the field test error (Islam et al. 2012).

In addition, the theoretical study of electrical resistivity has also attracted the attention of many researchers. Archie (1942) proposed an electrical resistivity model for cohesionless soil and pure sandstone, but it was assumed in the model that solid particles do not conduct electricity. Later, Waxman and Smits (1968), Rhoades and Schilfgaarde (1976), and Fortier et al. (2008) improved Archie's model from different perspectives and expanded its application scope. Based on the difference of three-phase conductivity of geotechnical materials (Fukue et al. 1999; Hasan et al. 2018; Yang et al. 2020), some researchers have theoretically deduced the conductivity model of geotechnical materials from the perspective of series and parallel connections (Fukue et al. 1999; Hasan et al. 2018; Tang et al. 2018). Shan et al. (2015) established a new model to characterize the electrical resistivity of frozen soils based on laboratorial tests and combined with the soil structure, and the new model was tested by the validation datasets from the four conditions (water, temperature, density, salt). Nevertheless, most of these studies involve empirical models and few theoretical models of electrical resistivity in loess have been proposed. Furthermore, there has been little research on electrical resistivity in the loess of northwest China.

The aims of this study were twofold: (i) to investigate the effects of moisture content and salt concentration on the electrical resistivity of loess from northwestern China and (ii) to propose a new loess electrical resistivity theoretical model comprised of simple parameters that consider the influences of moisture content and salt concentration. This result will (i) help to calibrate large-scale field-based electrical-resistivity datasets, (ii) provide a valuable reference for the prevention and control of environmental geo-crisis induced by groundwater changes in loess regions, (iii) obtain a basic data support to explore the environmental status of saline soils, and (iv) allow better utilization of soil resources in northwest China.

Materials and method

Materials

Materials tested in this research were Q_2 loess, which were collected from the south Jingyang platform on the southern edge of the Chinese Loess plateau (Fig. 1). Over 62 severe loess landslides occurred in this area since agricultural irrigation began in 1976 (Duan et al. 2021a, 2019; Ma et al. 2021). The loess samples in field were obtained about 17 m away from the ground surface. Its basic physical properties were determined following relevant standard methods (ASTM 2009), and results are presented in Table 1. Particle-size distribution of experimental loess in Fig. 2 was obtained using a laser particle size tester, which indicates that the loess is classified as a silty clay (ASTM-D2487 2017). The mineralogical composition and major chemical composition of loess were determined by an XRD and XRF respectively, and the results are listed in Tables 2 and 3. In addition, Table 3 represents that soluble salt of loess in this area is mainly NaCl, which is also widely mentioned in others' study (Duan et al. 2021b; Yan et al. 2021).

Sample preparation

The preparation of loess samples consisted of the following five steps: (1) the fresh loess was oven-dried at 110℃ for 12 h, subsequently grounded by a rubber hammer, and sieved through 2-mm sieve (Chen et al. 2020; Hu et al. 2021; Li et al. 2021a; Xu et al. 2021b); the above operations can remove organic matter and residual moisture; (2) dried loess was mixed with distilled water and sodium chloride to reach the target moisture content and salt concentration from Table 4, and the mass of distilled water, sodium chloride, and dried loess was calculated using the weighting method; (3) loess, distilled water, and NaCl were mixed by stirring for 10 min with the agitator and sealed in a double-layer plastic bag for 24 h on average 20℃ to homogenize the water (Lyu et al. 2020; Xue et al. 2021); (4) static compaction method can control the distance from hydraulic jack, and ensure each sample has the same volume, compactness, and density (Geng and Sun 2018; Melo et al. 2021). Then, the mixed

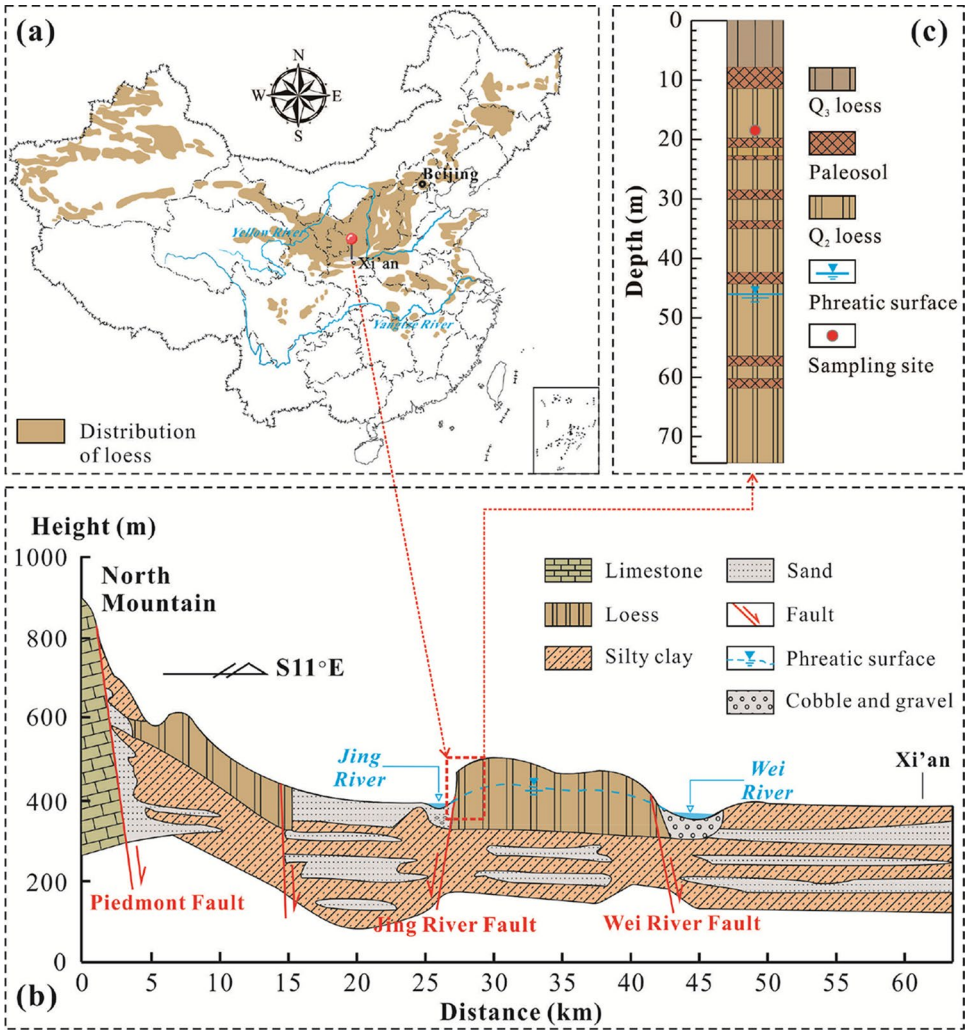

Fig. 1 Details of the study area and sampling site. (a) Distribution of Chinese Loess Plateau. (b) Environmental geo-condition in sampling site. (c) Loess profile at the sampling site

Table 1 Basic physical properties of the loess used in the experiment

Sample	Moisture content (%)	Dry density ($g \cdot cm^{-3}$)	Void ratio	Plastic limit (%)	Liquid limit (%)	Specific gravity
Loess	7.5	1.44	0.72	16.0	32.1	2.71
Standard deviation	0.10	0.20	0.02	0.5	0.5	0.3

loess was compacted in three layers by a hydraulic jack in the rigid mold (Islam et al. 2012; Wang et al. 2020). Finally, required loess sample was fabricated into a cylindrical specimen with a dry density of 1.70 $g \cdot cm^{-3}$ and dimensions of 39.1 mm × 30.0 mm; (5) the error of the sample size, moisture content, and NaCl concentration of all remold loess specimens should be controlled within 0.2% (Liu et al. 2021; Xu et al. 2021a). All specimens were placed in a constant temperature chamber before the test starts. The entire sample preparation procedure was carried out at room temperature to eliminate the influences of temperature on the experimental results.

Test methods

Existing measurement systems have certain disadvantages: the four-electrode resistivity measurement system disturbs soil structure (Shan et al. 2015), and the DC (direct current) method can change in moisture, pore-fluid chemistry, and soil structure that cause data scatter (Abu-Hassanein Zeyad et al. 1996). Therefore, the LCR digital bridge tester using two-electro resistivity measurement system and AC (alternating current) was used for this test (Fig. 3, Table 5). Two copper electrodes with a diameter of 40 mm and thickness of 2 mm were placed at the top and bottom

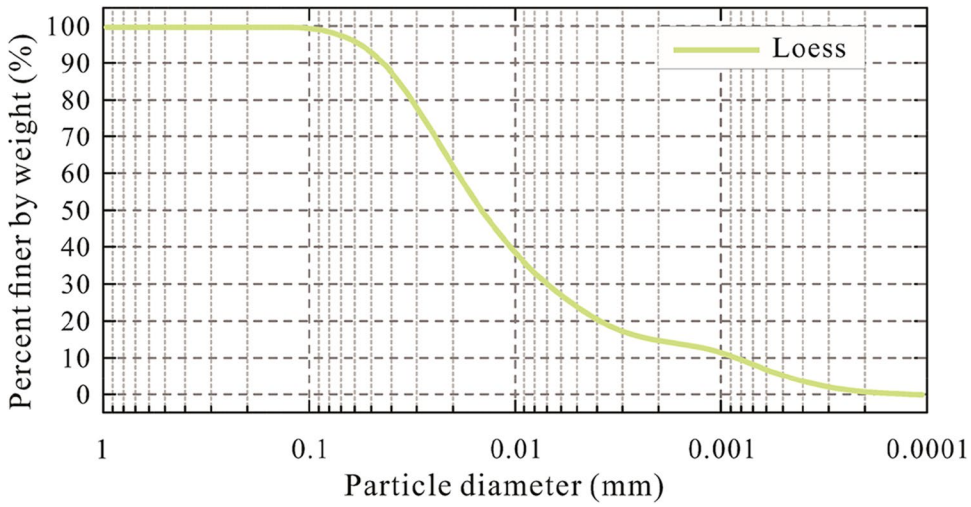

Fig. 2 Particle-size distribution curve for the loess used in the study

Table 2 Mineralogical composition of the loess used in the experiment

Item	Quartz	Carbonate	Illite	Kaolinite	Chlorite	Smectite	Others
Content (%)	28	23	21	3	16	6	3

Table 3 Major chemical composition of the loess used in the experiment

Item	Na^+	K^+	Mg^{2+}	Ca^{2+}	Cl^-	SO_4^{2-}
Content (g/kg)	42.42	0.58	2.39	12.82	40.26	14.61

Table 4 Moisture content and NaCl concentration of each sample in the test design scheme

Sample	1	2	3	4	5	6	7	8	9	10	11	12
Moisture content (%)	8	8	8	8	10	10	10	10	12	12	12	12
NaCl concentration (%)	0	2	4	6	0	2	4	6	0	2	4	6
Sample	13	14	15	16	17	18	19	20	21	22	23	24
Moisture content (%)	14	14	14	14	16	16	16	16	18	18	18	18
NaCl concentration (%)	0	2	4	6	0	2	4	6	0	2	4	6

Moisture content (w): the ratio of distilled water weight to weight of the dry loess; NaCl concentration (c): the ratio of sodium chloride weight to weight of the distilled water

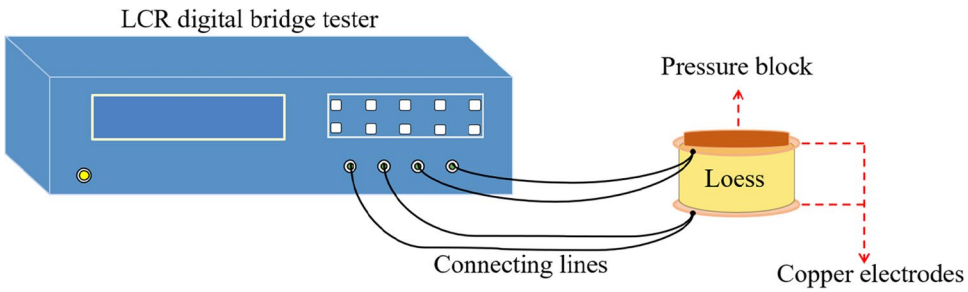

Fig. 3 LCR digital bridge instrument

Table 5 Equipment parameters of LCR digital bridge tester

Items	Parameters
Indices	L-Q, C-D, R-Q, |Z|-Q
Basic accuracy	0.2%
Frequency range (Hz)	100–10,000
Equivalent circuit	Serial and parallel connection
Output impedance (Ω)	30, 100
Trigger mode	Inside
Test signal level (Vrms)	0.3, 1
Measuring range	*R* (0.1 mΩ–99.99 MΩ); *C* (0.01 pF–99.99 μF); *L* (0.01 μH–99.99 μH); *Q* (0.0001–9999); *D* (0.0001–9.999)

of a cylindrical loess sample (Liu et al. 2008; Zhang et al. 2014) and connected to an experimental instrument. A pressure block was placed on the top of loess sample to ensure a well contact between the copper electrodes and loess samples (Muñoz-Castelblanco et al. 2012), which can effectively reduce the error (Muñoz-Castelblanco et al. 2012; Shah and Singh 2004). Before the test, open and circuit corrections were applied before conducting experiments and the authors calibrated the LCR tester according to the method of Shah and Singh (2004) and Tang et al. (2018). To eliminate the adverse effect of high frequencies and low frequencies on the electrical resistivity, three test frequencies (100 Hz, 1 kHz, 10 kHz) were used in this research (Duan et al. 2021b). Each loess sample was measured four times at each test frequency, and test results were averaged to minimize the test error. All of the measurements of the resistance were performed under the controlled temperature (20 ± 1°C). The electrical resistivity of loess is calculated based on the following equation:

$$\rho = R \bullet \frac{S}{L} \tag{1}$$

In which ρ = loess electrical resistivity (Ω·m); R = loess resistance measured by measuring (Ω); S = cross-section area through which electrical current conducts (m^2). L = height of the loess sample (m).

Results

Variation of loess electrical resistivity with moisture content

Figure 4 shows the variation of loess electrical resistivity with moisture content under the three test frequencies. It indicates that the reduction effect of moisture content on loess electrical resistivity plays a key role: with the increase of moisture content, the electrical resistivity values of loess decrease and finally tend to a minimum value. Loess electrical resistivity continues to decrease as the testing frequency grows. Furthermore, with increases in loess moisture content, the slope of electrical resistivity curve decreases. The characteristics of these curves indicate that the effect of water on the electrical resistivity of loess may be gradual. A detailed analysis is provided in the "Discussion" section.

Variation of loess electrical resistivity with NaCl concentration

The variation of loess electrical resistivity with different NaCl concentrations under the influence of test frequency is shown in Fig. 5. The effect of salt increases on the electrical resistivity of geo-materials has been mentioned in many studies (Lyu et al. 2019; Rhoades et al. 1989; Zhou et al. 2015). The electrical resistivity of loess is significantly higher at 0% NaCl than at other concentrations. Variations in electrical resistivity characteristics occurred at all moisture contents (from 8–20%). At higher NaCl concentrations of 2–6%, the electrical resistivity decreases overall but at a much lower rate than from 0–2% NaCl. Finally, the minimum electrical resistivity was reached at an NaCl concentration of 6%. The above interesting phenomenon indicates that there is an approximate critical content around 2% NaCl concentration (Duan et al. 2021b; Lyu et al. 2019).

Discussion

Electrical resistivity models of geo-materials have been systematically studied (Bai et al. 2013; Datsios et al. 2017); however, there are few studies on the loess electrical resistivity. In this study, combined with the three-phase path (Li et al. 2021b, 2020b; Tang et al. 2018) and diffuse double-layer structure (Darrow et al. 2020; Ruedrich et al. 2011), loess conductive models are shown in Fig. 6. Paths 1, 2, and 3 represent three conductive paths: (i) loess particle contact points (Kubliha et al. 2017), (ii) the alternating conductivity

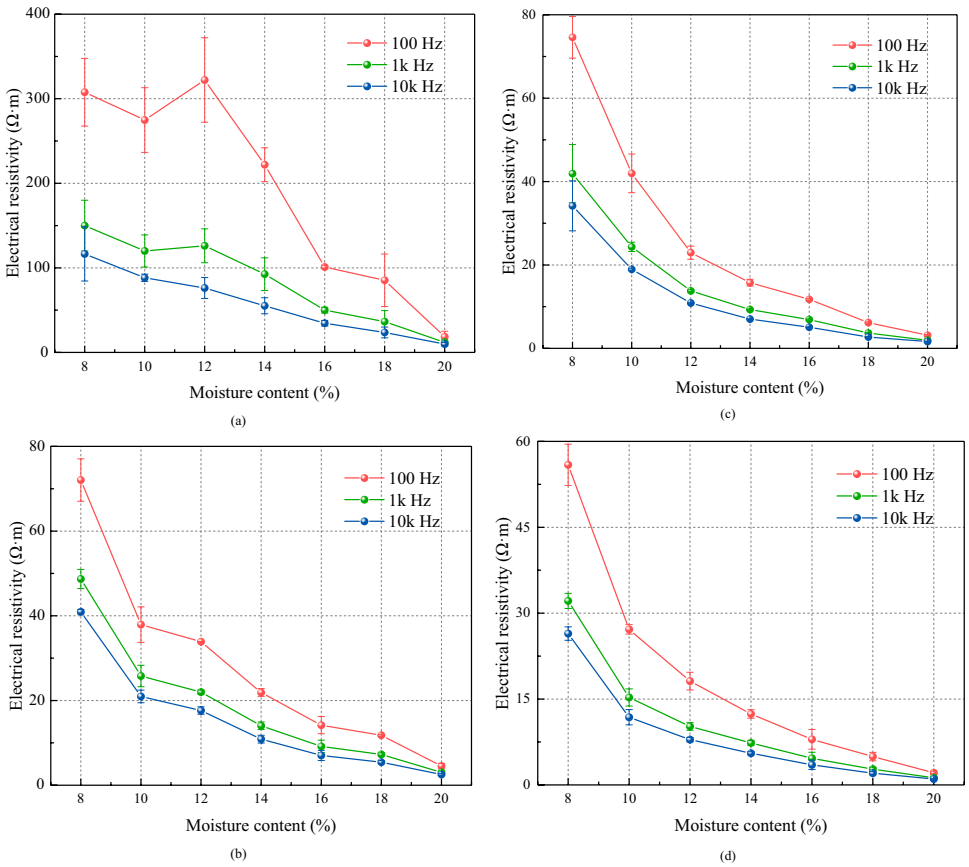

Fig. 4 Variations in the loess electrical resistivity with moisture content. **a** $c=0\%$; **b** $c=2\%$; **c** $c=4\%$; **d** $c=6\%$

of loess particles and pore water (Fukue et al. 1999; Hasan et al. 2018; Mojid et al. 2006), and (iii) continuous free pore water, respectively (You et al. 2020). The physical–chemical interactions between the electrically charged surface of loess particles (mainly clay particles) and the surrounding pore water form a diffuse double-layer structure that surrounds the loess particles, where both anions and cations have conductive capacity under electric field condition rather than insulating (Soga and Mitchell 2005). The above is shown in Figs. 6 and 7.

Influence of moisture content on loess electrical resistivity

At low moisture contents, the conductivity of loess is low, being almost equivalent to that of an insulator (Fukue et al. 1999). Combined with the three-phase path conduction model of loess, variation in the conductive paths in loess in relation to moisture content is shown in Fig. 6. Firstly, due to the lack of pore water, the single point contact mode of loess particles becomes the main conductive path (path 1). In fact, the electrical conductivity of loess particles is far less than that of pore water (Kubliha et al. 2017; Palacky 1987; Shevnin et al. 2007). Thereby, the electrical resistivity of loess in the initial stage is the greatest and is significantly higher than that at other moisture contents. Secondly, due to the increase of moisture content, some pores in loess are filled with water, the adverse effect of air on the formation of conductive path is reduced, and some path 2 begins to form. Finally, when moisture content exceeds the critical content, the conductive path 3 formed by continuous pore water gradually becomes the main conductive mode. Actually, the plastic limit (16.0%) of soil has been mentioned as a key critical content in many literatures (Fukue et al. 1999; Herring et al. 2019).

Influence of NaCl concentration on loess electrical resistivity

The movement of ions in pore water is the main cause of geomaterial conductivity (Yang et al. 2020). It has been found that as the salt concentration of pore water solution alters, the

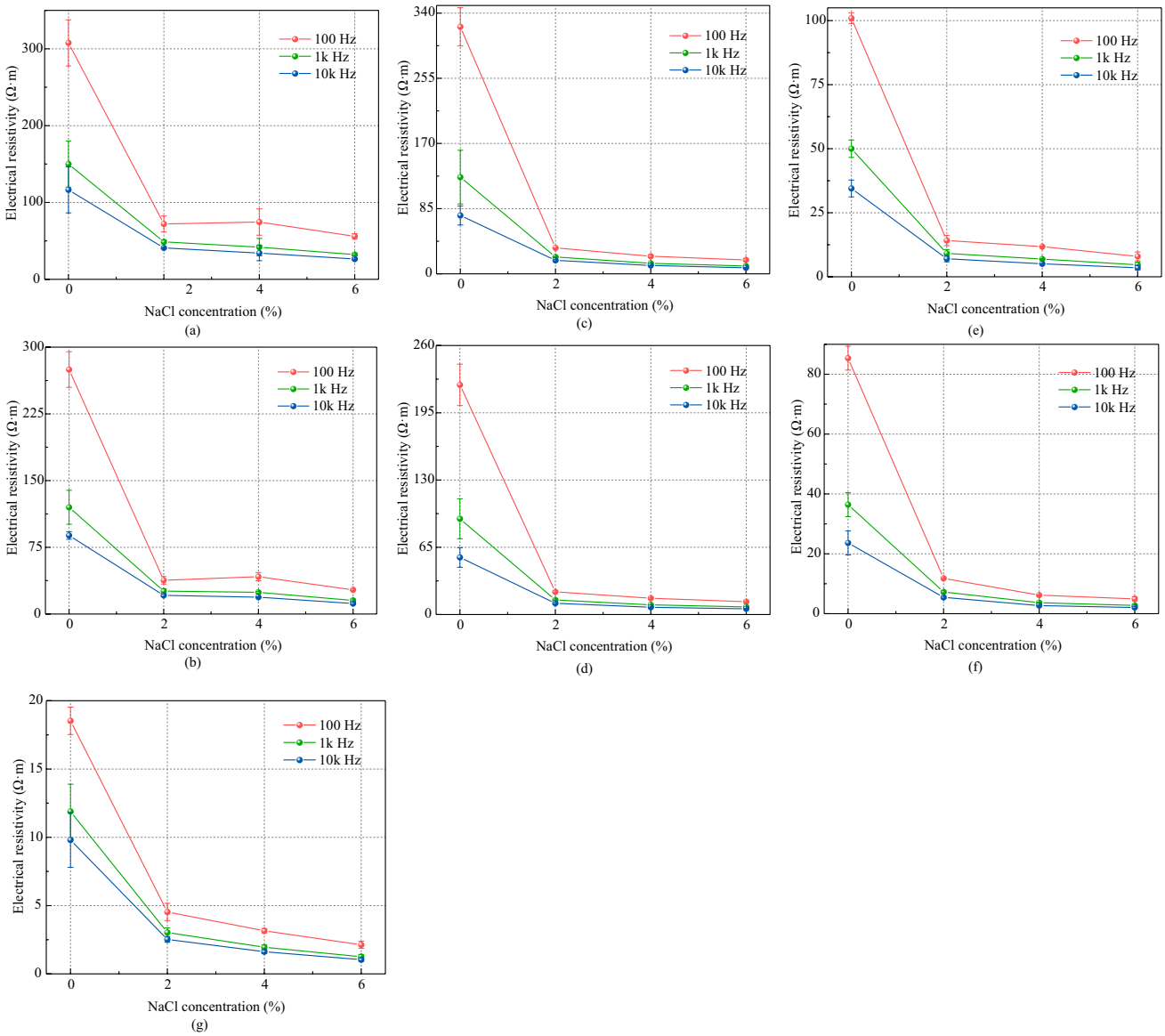

Fig. 5 Variations in the loess electrical resistivity with NaCl concentration. **a** $w = 8\%$; **b** $w = 10\%$; **c** $w = 12\%$; **d** $w = 14\%$; **e** $w = 16\%$; **f** $w = 18\%$; **g** $w = 20\%$

surface potential of soil particles will alter accordingly, which led to the changes in the thickness of the diffusion double layer of loess (Fig. 7) (Shevnin et al. 2007; Wang et al. 2019). When Na^+ and Cl^- added to the loess, under the influence of the external electric field, the diffuse double-layer properties (i.e., thickness, cation-exchange capacities, and counterion concentration) will change (Shevnin et al. 2007). The relatively free-moving ions from diffusion layer are more likely to produce directional movement to form conductive path under the action of external electric field, which is also the main reason for the significant decrease of loess electrical resistivity after the increase of salinity. In addition, as the pores of loess are gradually occupied by salt water, some salts and minerals gradually decompose in the pore water, which is beneficial to current transfer (Yang et al. 2020). The conductive path is formed by a large number of free-moving ions in the diffusion layer of clay particles and its surrounding pore water under the action of external electric field. Simultaneously, softening and melting

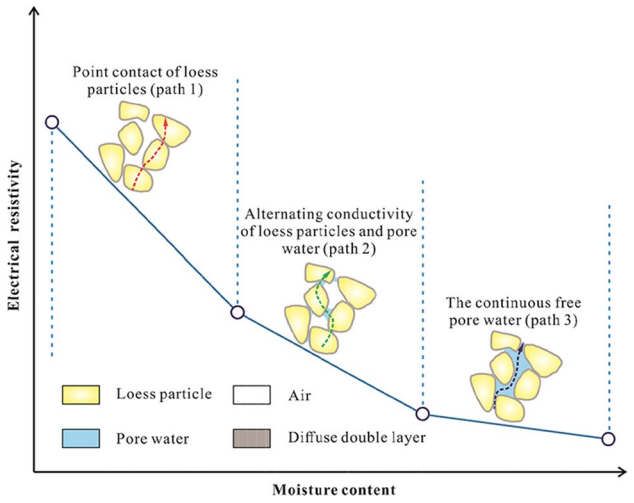

Fig. 6 Conceptual diagram of loess conductive path with different moisture content. The red, green and blue arrows represent paths 1, 2, and 3 respectively (Al Rashid et al. 2018; Choo et al. 2016)

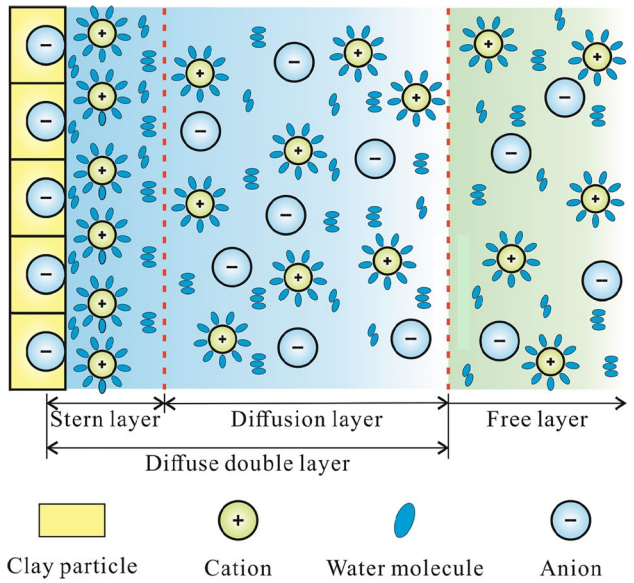

Fig. 7 Structural diagram of the diffuse double layer in loess (Chen et al. 2019; Darrow et al. 2020; Rinaldi Victor and Cuestas German 2002)

of soil particles due to chemical reactions around the pore walls not only expands the pores in the loess, which facilitates the connection of pore water, but also releases free-moving ions that contribute to the conductivity of the conductive path. Thereby, in this stage (c is from 2 to 6%), the electrical resistivity of loess decreases continuously.

Theoretical model and calculations

Theoretical model

Model of loess electrical resistivity under the influence of moisture content

Conduction in loess involves two different processes: (i) pore water in the gaps between loess particles and (ii) the diffuse double layer around the clay surfaces. These processes are closely related to the moisture content, NaCl concentration, and porosity of loess. Figure 8 shows the three-phase conductive system of the loess, where the electrical resistivity is the result of interactions between the pore water, loess particles, and loess structure (Fukue et al. 1999).

Firstly, the following assumptions are made based on the three-phase conductive system of the loess and simplified circuit diagram in Fig. 8.

$$L_s + L_w + L_a + L_1 = 1 \tag{2}$$

$$L_{s1} + L_{w1} = 1 \tag{3}$$

Series and parallel connections are used to characterize the complex connection among three components in soil (Ellis et al. 2010; Mojid et al. 2006). Therefore, the loess electrical resistivity is expressed as:

$$\frac{1}{R_1} + \frac{1}{R_s} + \frac{1}{R_w} + \frac{1}{R_{s1} + R_{w1}} \tag{4}$$

where R_1 represents the loess resistance under the influence of moisture content. According to the electrical resistivity calculation equation ($R = \rho L/$), the following equations are obtained:

$$R_s = \rho_s L_s \tag{5}$$

$$R_w = \rho_w L_w \tag{6}$$

$$R_{s1} = \frac{\rho_s L_1}{L_{s1}} \tag{7}$$

$$R_{w1} = \frac{\rho_w L_1}{L_{w1}} \tag{8}$$

After, the following definitions are given:

$$\alpha_1 = \frac{R_{s1}}{R_s} \tag{9}$$

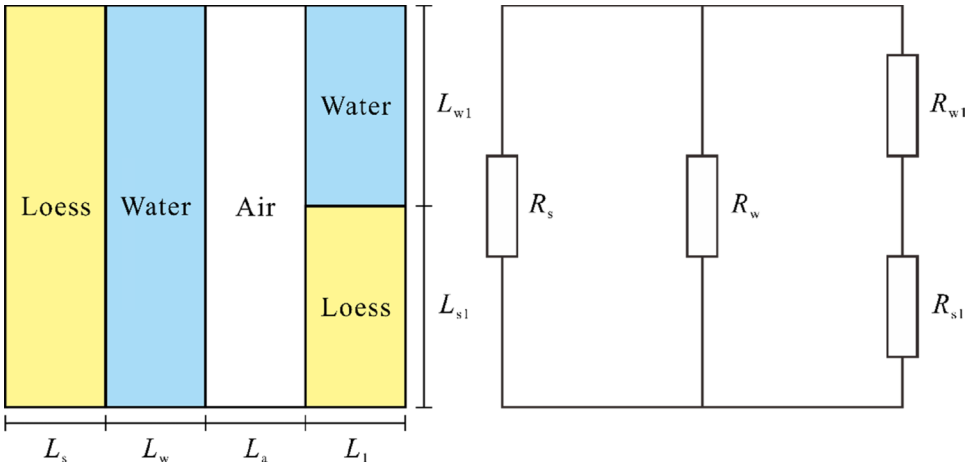

(a) Loess conductivity model diagram (b) Simplified circuit diagram

Fig. 8 Schematic diagram of the loess conductivity model with moisture content. **a** Loess conductivity model diagram; **b** simplified circuit diagram

$$\beta_1 = \frac{R_{w1}}{R_w} \tag{10}$$

Thereby, the following equation can be obtained:

$$\frac{1}{R_1} = \frac{2\alpha_1 + 2\beta_1 + 1}{\beta_1 \rho_s L_s + \alpha_1 \rho_w L_w} \tag{11}$$

Loess electrical resistivity is closely related to the diffusion double-layer structure around the soil particles. Therefore, the conductivity of diffusion double layer is introduced into Eq. 11 to simplify the model (Waxman and Smits 1968). There is a power function relationship between the electrical resistivity of pore water and moisture content. The simplification process takes into account the diffusion double-layer structure and cation exchange capacities (CEC). Finally, the electrical resistivity model of loess affected by moisture content is as follows:

$$\rho_1 = \frac{a_1}{b_1 + c_1 w^{\theta}} \tag{12}$$

where ρ_1 represents the loess electrical resistivity (Ω·m); w represents the loess moisture content; $a_1 = 2\alpha_1 + 2\beta_1 + 1$ is the soil structure parameter; $b_1 = \beta_1 \rho_s L_s$ represents the conductivity parameter of diffuse double layer; c_1 and θ represent the resistance parameter under the influence of loess moisture content.

Loess electrical resistivity model under the influence of NaCl concentration

The increased NaCl concentration in pore water allows the entire conductive loess to be regarded as a mixed conductive

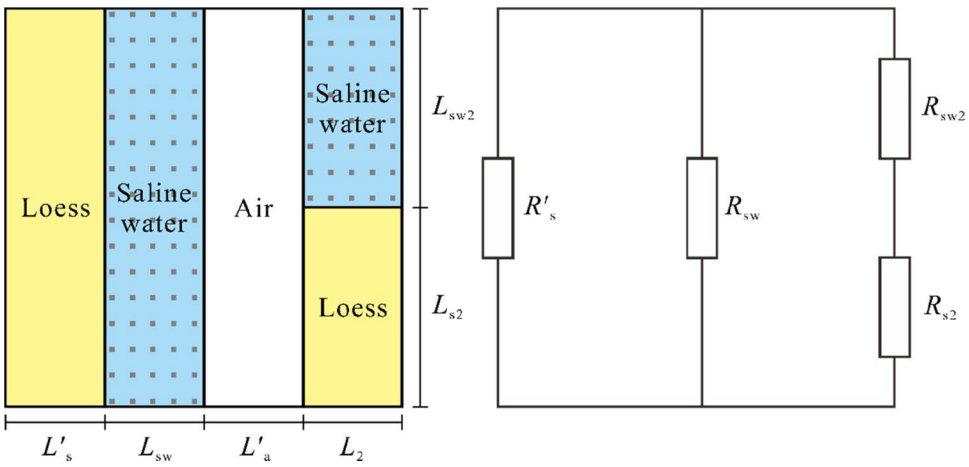

(a) Loess conductivity model diagram (b) Simplified circuit diagram

Fig. 9 Schematic diagram of the loess conductivity model with NaCl concentration. **a** Loess conductivity model diagram; **b** simplified circuit diagram

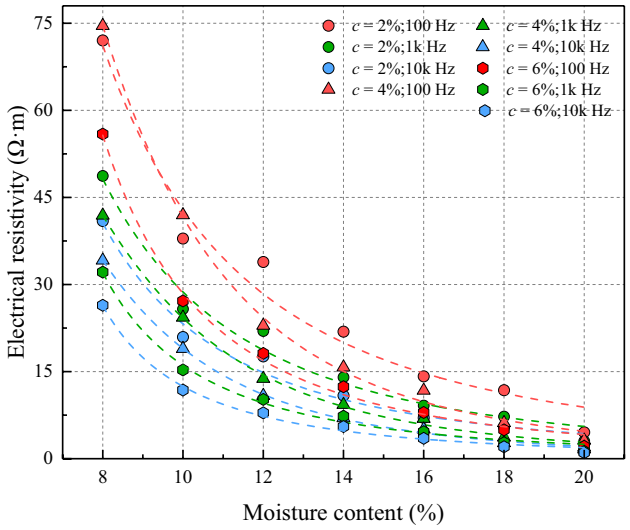

Fig. 10 Validation results for the electrical resistivity model affected by moisture content based on experimental data

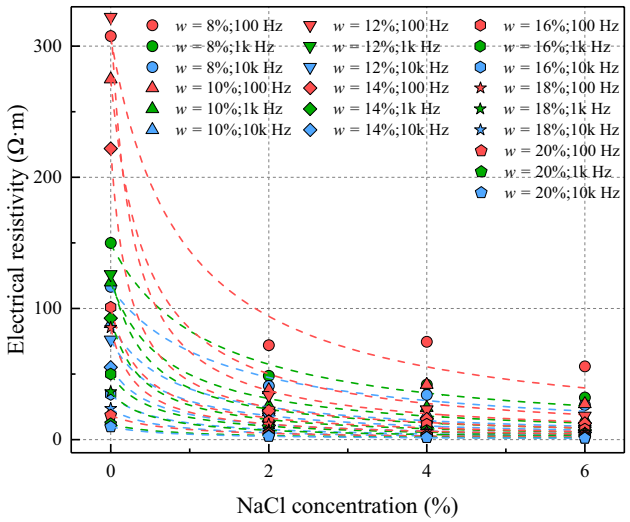

Fig. 11 Validation results for the electrical resistivity model affected by NaCl concentration based on experimental data

body as caused by solid-phase loess particles, liquid-phase saline water, and air-phase void air, as shown in Fig. 9. Therefore, according to the loess electrical resistivity model derivation for the moisture content condition in the "Model of loess electrical resistivity under the influence of moisture content" section, this research provides the following assumptions:

$$L_s^{'} + L_{sw} + L_a^{'} + L_2 = 1 \tag{13}$$

$$L_{s2} + L_{sw2} = 1 \tag{14}$$

$$\frac{1}{R_2} = \frac{1}{R_s^{'}} + \frac{1}{R_{sw}} + \frac{1}{R_{s2} + R_{sw2}} \tag{15}$$

$$R_s^{'} = \rho_s L_s^{'} \tag{16}$$

$$R_{sw} = \rho_{sw} L_{sw} \tag{17}$$

$$R_{sw2} = \frac{\rho_{sw} L_2}{L_{sw2}} \tag{18}$$

where R_2 represents the loess resistance under influence of NaCl concentration.

$$\beta_2 = \frac{R_{sw2}}{R_{sw}} \tag{19}$$

Therefore, the following equation was concluded:

$$\frac{1}{R_2} = \frac{2\alpha_2 + 2\beta_2 + 1}{\beta_2 \rho_s L_s^{'} + \alpha_2 \rho_{sw} L_{sw}} \tag{20}$$

When the loess has a high NaCl concentration, most of the pore water is full of freely moving conductive ions. Pore water can be regarded as a conductive unit closely related to NaCl concentration. Therefore, the equation for loess electrical resistivity is deduced as:

Table 6 Validation results for electrical resistivity model affected by moisture content based on experimental data

NaCl concentration (%)	Test frequency (Hz)	a_1	b_1	c_1	θ	R-squared values
2	100	1313.500	0.168	0.159	2.281	0.975
2	1 k	814.600	1.234	0.147	2.393	0.984
2	10 k	1090.700	0.930	0.148	2.400	0.981
4	100	4961.100	19.370	0.043	3.369	0.998
4	1 k	2677.900	22.770	0.345	3.400	0.998
4	10 k	19,073.000	161.300	0.350	3.382	0.998
6	100	1843.000	5.755	0.150	2.672	0.995
6	1 k	713.640	6.856	0.150	2.533	0.994
6	10 k	460.950	9.669	0.173	2.431	0.995

Table 7 Validation results for electrical resistivity model affected by NaCl concentration based on experimental data

Moisture content (%)	Test frequency (Hz)	a_2	b_2	c_2	*R*-squared values
8	100	5.866	0.019	0.216	0.974
8	1 k	56.004	0.375	0.300	0.983
8	10 k	64.155	0.554	0.400	0.984
10	100	5.233	0.019	0.042	0.990
10	1 k	3.067	0.026	0.036	0.990
10	10 k	2.624	0.030	0.038	0.990
12	100	4.984	0.015	0.059	0.990
12	1 k	2.502	0.200	0.440	0.990
12	10 k	2.933	0.039	0.061	0.990
14	100	5.340	0.024	0.097	0.990
14	1 k	3.240	0.035	0.088	0.990
14	10 k	3.851	0.070	0.130	0.990
16	100	4.058	0.040	0.103	0.990
16	1 k	3.691	0.074	0.143	0.990
16	10 k	3.311	0.096	0.166	0.990
18	100	3.712	0.043	0.134	0.990
18	1 k	3.342	0.092	0.190	0.990
18	10 k	2.067	0.087	0.152	0.990
20	100	2.466	0.133	0.187	0.990
20	1 k	2.226	0.187	0.262	0.990
20	10 k	1.989	0.203	0.281	0.990

$$\rho_2 = \frac{a_2}{b_2 + c_2 c} \tag{21}$$

where ρ_2 represents the loess electrical resistivity; c represents the NaCl concentration; $a_2 = 2a_2 + 2\beta_2 + 1$ represents the loess structural parameter under the influence of NaCl concentration; $b_2 = \beta_2 \rho_s L_s^{'}$ represents the conductive parameter of the diffuse double layer, and c_2 represents the coefficient under the influence of NaCl concentration.

Calculation and verification

Data from the loess electrical resistivity experiment were used to evaluate the proposed model. The fitting results under the influence of moisture content and NaCl concentration are shown in Figs. 10 and 11, respectively. Deterministic coefficient (R^2) was used to evaluate the loess electrical resistivity model, and the result of model validation is shown in Tables 6 and 7. The determination coefficient represents the difference between the experimental results and the theoretical calculation results, and its value is between 0 and 1. The larger the value is, the stronger the adaptability of the model is (Wang and Hayakawa 1993; Yun et al. 2013). The high degree of similarity between the experimental data and the theoretical data in Figs. 10 and 11 and the expected deterministic coefficient from Tables 6 and 7 show that the

Table 8 Validation results for new models based on the collected data from different types of soil

Number	Sample name	References	Location	*R*-squared values	
				Moisture content	NaCl concentration
1	Cheshire clay	McCarter (1984)	Cheshire, UK	0.974	
2	London clay	McCarter (1984)	London, UK	0.969	
3	Loamy clay	Michot et al. (2003)	Paris, France	0.990	
4	Type-a Wuhan clay	Hu et al. (2019)	Wuhan, China	0.990	
5	Type-b Wuhan clay	Hu et al. (2019)	Wuhan, China	0.997	
6	Yanan loess	Nie et al. (2021)	Yanan, China	0.992	
7	Type a-marine clay	Zhang et al. (2014)	Lianyungang, China		0.895
8	Type b-marine clay	Zhang et al. (2014)	Lianyungang, China		0.983
9	Type c-marine clay	Zhang et al. (2014)	Lianyungang, China		0.810
10	Sheyang clay	Zhang et al. (2018)	Sheyang, China		0.934
11	Yancheng clay	Zhang et al. (2018)	Yancheng, China		0.979
12	NaCl-a Yangling loess	Luo et al. (2019)	Yangling China		0.997
13	NaCl-b Yangling loess	Luo et al. (2019)	Yangling China		0.956
14	Na_2CO_3-a Yangling loess	Luo et al. (2019)	Yangling China		0.993
15	Na_2CO_3-b Yangling loess	Luo et al. (2019)	Yangling China		0.938
16	Na_2SO_4-a Yangling loess	Luo et al. (2019)	Yangling China		0.984
17	Na_2SO_4-b Yangling loess	Luo et al. (2019)	Yangling China		0.893

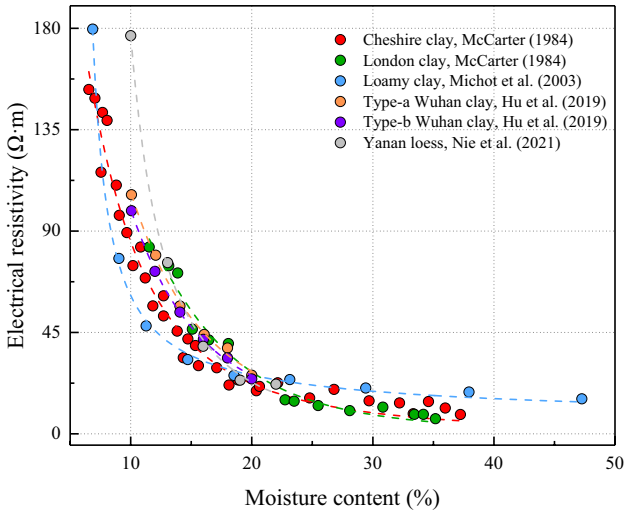

Fig. 12 Validation results for the electrical resistivity model affected by moisture content based on collected data

loess electrical resistivity model proposed in this study has good applicability.

In addition, soil electrical resistivity data from different types of researches around the world were collected to evaluate the new models (Table 8; Hu et al. 2019; Luo et al. 2019; McCarter 1984; Michot et al. 2003; Nie et al. 2021; Zhang et al. 2014, 2018). Figures 12 and 13 show the results of fitting the collected data with Eq. 11 and Eq. 21, respectively. The better results between the measured values and the theoretical values, and the high deterministic coefficient, show that the new model has strong applicability.

Conclusions

The influences of moisture content and NaCl concentration on the electrical resistivity of loess from the south Jingyang Platform, Shaanxi Province, in the Loess Plateau of Northwest China were studied by an LCR digital bridge instrument with three test frequencies. The following conclusions were obtained:

(1) Test results present the plastic limit (16%) and around 2% NaCl concentration are the critical content of loess electrical resistivity that affected the moisture content and NaCl concentration, respectively. Experimental values gradually decrease and tend to a minimum value after exceeding the critical content.

(2) The influence of moisture content on the loess electrical resistivity is mainly reflected in the change of the contact model between soil particles and the change of conductive path. As the main factor affecting the number of free-moving ions in pore water, NaCl concentration modifies the conductive ability of conductive path.

(3) Based on the three-phase composition of loess and the diffuse double-layer structure around the solid particles, new models that consider the influence of moisture content and NaCl concentration show good applicability in the experimental data from various countries and regions.

(4) In addition, the complexity of site conditions requires researchers to conduct more in-depth studies, such as the relationship between the engineering mechanical properties, water sensitivity, thermal conductivity, soil chemical properties, and electrical resistivity.

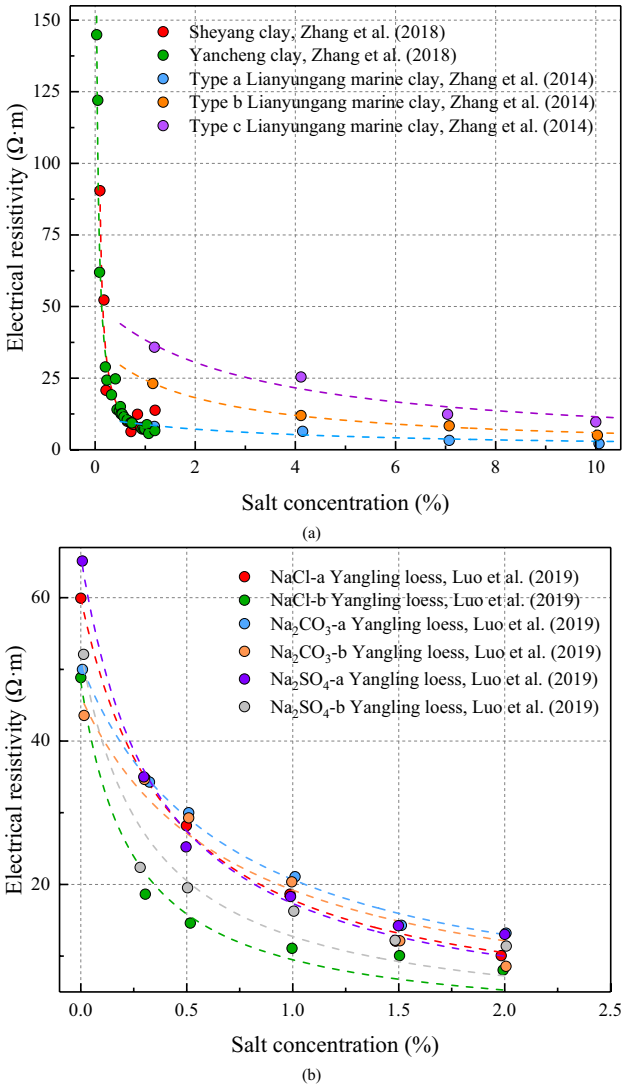

Fig. 13 Validation results for the electrical resistivity model affected by NaCl concentration based on collected data. **a** Clay. **b** Loess

Acknowledgements The authors thank Dr. Heng Li and Dr. Chenxi Dong for writing guidance and review services. We also thank Mr. He Zhang and Dr. Zhenlong Ge who collaborated in the experimental process and proposed the valuable suggestion about this study.

Author contribution Zhao Duan: funding acquisition, resources, writing—review and editing. Xusheng Yan: conceptualization, methodology, software, investigation, writing—original draft. Qiang Sun: funding acquisition, project administration, resources, supervision. Xuan Tan: data curation, visualization, validation. Xin Chen: writing—review and editing; formal analysis.

Funding This work was supported by the Natural Science Foundation of China (grant nos. 42177155, 41790442, and 41972288) and the China Postdoctoral Science Foundation (grant no. 2020M683676XB).

Data availability All data generated or analyzed during this study are included in this published article.

Declarations

Ethics approval and consent to participate Not applicable.

Consent for publication The authors declare that they consent for the publication of this study.

Competing interests The authors declare no competing interests.

References

Abu-Hassanein Zeyad S, Benson Craig H, Blotz Lisa R (1996) Electrical resistivity of compacted clays. J Geotech Eng 122:397–406. https://doi.org/10.1061/(ASCE)0733-9410(1996)122:5(397)

Al Rashid QA, Abuel-Naga HM, Leong EC, Lu Y, Al Abadi H (2018) Experimental-artificial intelligence approach for characterizing electrical resistivity of partially saturated clay liners. Appl Clay Sci 156:1–10. https://doi.org/10.1016/j.clay.2018.01.023

Archie GE (1942) The electrical resistivity log as an aid in determining some reservoir characteristics. Trans AIME 146:54–62. https://doi.org/10.2118/942054-G

ASTM-D2487 (2017) Standard practice for classification of soils for engineering purposes (Unified Soil Classification System). West Conshohocken. https://doi.org/10.1520/D2487-17E01

ASTM (2009) Annual book of ASTM standards. West Conshohocken

Bai W, Kong LW, Guo AG (2013) Effects of physical properties on electrical conductivity of compacted lateritic soil. J Rock Mech Geotech Eng 5:406–411. https://doi.org/10.1016/j.jrmge.2013.07.003

Cai JC, Wei W, Hu XY, Wood DA (2017) Electrical conductivity models in saturated porous media: a review. Earth Sci Rev 171:419–433. https://doi.org/10.1016/j.earscirev.2017.06.013

Cardoso R, Dias AS (2017) Study of the electrical resistivity of compacted kaolin based on water potential. Eng Geol 226:1–11. https://doi.org/10.1016/j.enggeo.2017.04.007

Chang WB, Wang P, Hj W, Chai Sf Yu, Sy YX (2021a) Simulation of the Q2 loess slope with seepage fissure failure and seismic response via discrete element method. Bull Eng Geol Env 80:3495–3511. https://doi.org/10.1007/s10064-021-02139-z

Chang WB, Xing AG, Wang P, Zhuang Y, Jin KP, He JY, Chai SF (2021b) Analysis of Dangchuan 5# landslide on January 27, 2021, in Yongjing County, Gansu Province, China. Landslides. https://doi.org/10.1007/s10346-021-01743-0

Chen J, Fang YG, Gu RG, Shu HK, Ba LZ, Li W (2019) Study on pore size effect of low permeability clay seepage. Arab J Geosci 12:238. https://doi.org/10.1007/s12517-019-4375-3

Chen X, Li J, Xue Q, Huang X, Liu L, Poon CS (2020) Sludge biochar as a green additive in cement-based composites: mechanical properties and hydration kinetics. Constr Build Mater 262:120723. https://doi.org/10.1016/j.conbuildmat.2020.120723

Choo H, Song J, Lee W, Lee C (2016) Impact of pore water conductivity and porosity on the electrical conductivity of kaolinite. Acta Geotech 11:1419–1429. https://doi.org/10.1007/s11440-016-0490-4

Chu Y, Liu S, Bate B, Xu L (2018) Evaluation on expansive performance of the expansive soil using electrical responses. J Appl Geophys 148:265–271. https://doi.org/10.1016/j.jappgeo.2017.12.001

Darrow MM, Guo R, Trainor TP (2020) Zeta potential of cation-treated soils and its implication on unfrozen water mobility. Cold Reg Sci Technol 173:103029. https://doi.org/10.1016/j.coldregions.2020.103029

Datsios ZG, Mikropoulos PN, Karakousis I (2017) Laboratory characterization and modeling of DC electrical resistivity of sandy soil with variable water resistivity and content. IEEE Trans Dielectr Electr Insul 24:3063–3072. https://doi.org/10.1109/TDEI.2017.006583

De Jong SM, Heijenk RA, Nijland W, van der Meijde M (2020) Monitoring soil moisture dynamics using electrical resistivity tomography under homogeneous field conditions. Sensors 20.https://doi.org/10.3390/s20185313

Doetsch J, Linde N, Vogt T, Binley A, Green AG (2012) Imaging and quantifying salt-tracer transport in a riparian groundwater system by means of 3D ERT monitoring. Geophysics 77:B207–B218. https://doi.org/10.1190/geo2012-0046.1

Duan Z, Cheng W-C, Peng J-B, Rahman MM, Tang H (2021a) Interactions of landslide deposit with terrace sediments: perspectives from velocity of deposit movement and apparent friction angle. Eng Geol 280:105913. https://doi.org/10.1016/j.enggeo.2020.105913

Duan Z, Cheng WC, Peng JB, Wang QY, Chen W (2019) Investigation into the triggering mechanism of loess landslides in the south Jingyang platform, Shaanxi province. Bull Eng Geol Env 78:4919–4930. https://doi.org/10.1007/s10064-018-01432-8

Duan Z, Wu YB, Tang H, Ma JQ, Zhu XH (2020) An analysis of factors affecting flowslide deposit morphology using taguchi method. Advances in Civil Engineering 2020:8844722. https://doi.org/10.1155/2020/8844722

Duan Z, Yan X, Sun Q, Tan X, Dong C (2021b) Effects of water content and salt content on electrical resistivity of loess. Environmental Earth Sciences 80:469. https://doi.org/10.1007/s12665-021-09769-2

Ellis M, Sinha M, Minshull T, Sothcott J, Best A (2010) An anisotropic model for the electrical resistivity of two-phase geologic materials. Geophysics 75.https://doi.org/10.1190/1.3483875

Erzin Y, Rao B, Patel A, Gumaste S, Singh D (2010) Artificial neural network models for predicting electrical resistivity of soils from their thermal resistivity. Int J Therm Sci 49:118–130. https://doi.org/10.1016/j.ijthermalsci.2009.06.008

Fan XM, Xu Q, Scaringi G, Li S, Peng DL (2017) A chemo-mechanical insight into the failure mechanism of frequently occurred landslides in the Loess Plateau, Gansu Province. China Engineering Geology 228:337–345. https://doi.org/10.1016/j.enggeo.2017.09.003

Fortier R, LeBlanc AM, Allard M, Buteau S, Calmels F (2008) Internal structure and conditions of permafrost mounds at Umiujaq in Nunavik, Canada, inferred from field investigation and electrical resistivity tomography. Can J Earth Sci 45:367–387. https://doi.org/10.1139/E08-004

Fu JT, Hu XS, Li XL, Yu DM, Liu YB (2019) Influences of soil moisture and salt content on loess shear strength in the Xining Basin, northeastern Qinghai-Tibet Plateau. J Mt Sci 16:1184–1197. https://doi.org/10.1007/s11629-018-5206-9

Fukue M, Minato T, Horibe H, Taya N (1999) The micro-structures of clay given by resistivity measurements. Eng Geol 54:43–53. https://doi.org/10.1016/S0013-7952(99)00060-5

Geng JS, Sun Q (2018) Effects of high temperature treatment on physical-thermal properties of clay. Thermochim Acta 666:148–155. https://doi.org/10.1016/j.tca.2018.06.018

Hasan M, Shang YJ, Jin WJ, Akhter G (2019) Investigation of fractured rock aquifer in South China using electrical resistivity tomography and self-potential methods. J Mt Sci 16:850–869. https://doi.org/10.1007/s11629-018-5207-8

Hasan MF, Abuel Naga H, Broadbridge P, Leong EC (2018) Series-parallel structure-oriented electrical conductivity model of saturated clays. Appl Clay Sci 162:239–251. https://doi.org/10.1016/j.clay.2018.06.020

Hen Jones R, Hughes P, Glendinning S, Gunn DA, Chambers J, Wilkinson P, Uhlemann S (2014) Determination of moisture content and soil suction in engineered fills using electrical resistivity. In: Unsaturated Soils: Research & Applications. CRC Press, pp 1695–1699. http://dx.doi.org/https://doi.org/10.1201/b17034-247

Herring T, Cey E, Pidlisecky A (2019) Electrical resistivity of a partially saturated porous medium at subzero temperatures. Vadose Zone Journal 18:190019. https://doi.org/10.2136/vzj2019.02.0019

Hu W, Cheng W, Wen S, Mizanur Rahman M (2021) Effects of chemical contamination on microscale structural characteristics of intact loess and resultant macroscale mechanical properties. CATENA 203:105361. https://doi.org/10.1016/j.catena.2021.105361

Hu Z, Peng K, Li L, Ma Q, Xiao H, Li Z, Ai P (2019) Effect of wetting-drying cycles on mechanical behaviour and electrical resistivity of unsaturated subgrade soil. Advances in Civil Engineering 2019:3465327. https://doi.org/10.1155/2019/3465327

Islam T, Chik Z, Mustafa MM, Sanusi H (2012) Modeling of electrical resistivity and maximum dry density in soil compaction measurement. Environmental Earth Sciences 67:1299–1305. https://doi.org/10.1007/s12665-012-1573-7

Joel ES, Olasehinde PI, Adagunodo TA, Omeje M, Akinyemi ML, Ojo JS (2019) Integration of aeromagnetic and electrical resistivity imaging for groundwater potential assessments of coastal plain sands area of Ado-Odo/Ota in southwest Nigeria. Groundw Sustain Dev 9:100264. https://doi.org/10.1016/j.gsd.2019.100264

Kemna A, Vanderborght J, Kulessa B, Vereecken H (2002) Imaging and characterisation of subsurface solute transport using electrical resistivity tomography (ERT) and equivalent transport models. J Hydrol 267:125–146. https://doi.org/10.1016/S0022-1694(02)00145-2

Kubliha M, Trnovcová V, Ondruška J, Štubňa I, Bošák O, Kaljuvee T (2017) Comparison of dehydration in kaolin and illite using DC conductivity measurements. Appl Clay Sci 149:8–12. https://doi.org/10.1016/j.clay.2017.08.012

Li C, Gao X, Li S, Bundschuh J (2020a) A review of the distribution, sources, genesis, and environmental concerns of salinity in groundwater. Environ Sci Pollut Res 27:41157–41174. https://doi.org/10.1007/s11356-020-10354-6

Li J, Wang Q, Chen Z, Xue Q, Chen X, Mu Y, Poon CS (2021a) Immobilization of high-Pb contaminated soil by oxalic acid activated incinerated sewage sludge ash. Environ Pollut 284:117120. https://doi.org/10.1016/j.envpol.2021.117120

Li K, Li D, Chen D, Gu S, Liu Y (2021b) A generalized model for effective thermal conductivity of soils considering porosity and mineral composition. Acta Geotech. https://doi.org/10.1007/s11440-021-01282-x

Li K, Li D, Liu Y (2020b) Meso-scale investigations on the effective thermal conductivity of multi-phase materials using the finite element method. Int J Heat Mass Transf 151:119383. https://doi.org/10.1016/j.ijheatmasstransfer.2020.119383

Liu K, Ye W, Jing H (2021) Shear strength and microstructure of intact loess subjected to freeze-thaw cycling. Adv Mater Sci Eng 2021:1173603. https://doi.org/10.1155/2021/1173603

Liu SY, Du YJ, Han LH, Gu MF (2008) Experimental study on the electrical resistivity of soil–cement admixtures. Environ Geol 54:1227–1233. https://doi.org/10.1007/s00254-007-0905-5

Liu Z, Liu S, Ma X, Wu C (2014) Electrical resistivity behavior of loess specimens during unconfined compression test. Paper presented at the Geo-Hubei 2014 International Conference on Sustainable Civil Infrastructure,

Luo S, Yang X, Fan H, Du Y (2019) Study on electrical resistivity characteristics of sodium salt saline soil. Water Power 45:22–26

Lyu C, Sun Q, Zhang W, Hao S (2019) Effects of NaCl concentration on electrical resistivity of clay with cooling. J Appl Geophys 170:103843. https://doi.org/10.1016/j.jappgeo.2019.103843

Lyu C, Sun Q, Zhang WQ (2020) Effects of NaCl concentration on thermal conductivity of clay with cooling. Bull Eng Geol Env 79:1449–1459. https://doi.org/10.1007/s10064-019-01624-w

Ma J, Zhao X, Li S, Duan Z (2021) Effects of high shearing rates on the shear behavior of saturated loess using ring shear tests. Geofluids 2021:6527788. https://doi.org/10.1155/2021/6527788

McCarter WJ (1984) The electrical resistivity characteristics of compacted clays. Géotechnique 34:263–267. https://doi.org/10.1680/geot.1984.34.2.263

Melo LBBd, Silva BM, Peixoto DS, Chiarini TPA, de Oliveira GC, Curi N (2021) Effect of compaction on the relationship between electrical resistivity and soil water content in Oxisol. Soil and Tillage Research 208:104876. https://doi.org/10.1016/j.still.2020.104876

Michot D, Benderitter Y, Dorigny A, Nicoullaud B, King D, Tabbagh A (2003) Spatial and temporal monitoring of soil water content with an irrigated corn crop cover using surface electrical resistivity tomography. Water Resour Res 39.https://doi.org/10.1029/2002WR001581

Mojid MA, Rose DA, Wyseure GCL (2006) A model incorporating the diffuse double layer to predict the electrical conductivity of bulk soil. Eur J Soil Sci 58:560–572. https://doi.org/10.1111/j.1365-2389.2006.00831.x

Muñoz-Castelblanco JA, Pereira JM, Delage P, Cui YJ (2012) The influence of changes in water content on the electrical resistivity of a natural unsaturated loess. Geotech Test J 35:11–17. https://doi.org/10.1520/GTJ103587

Nie Y, Ni W, Wang H, Yuan K, Tuo W, Li X (2021) Evaluation of collapsibility of compacted loess based on resistivity index. Adv Mater Sci Eng 2021:9990012. https://doi.org/10.1155/2021/9990012

Ozcep F, Yildirim E, Tezel O, Asci M, Karabulut S (2010) Correlation between electrical resistivity and soil-water content based artificial intelligent techniques. International Journal of Physical Sciences 5:47–56. https://doi.org/10.5897/IJPS.9000144

Palacky GJ (1987) Clay mapping using electromagnetic methods. First Break 5.https://doi.org/10.3997/1365-2397.1987015

Park J, Lee KH, Seo H, Ryu J, Lee IM (2017) Role of induced electrical polarization to identify soft ground/fractured rock conditions. J Appl Geophys 137:63–72. https://doi.org/10.1016/j.jappgeo.2016.12.017

Rhoades J, Schilfgaarde J (1976) An electrical conductivity probe for determining soil salinity1. Soil Sci Soc Am J - SSSAJ 40.https://doi.org/10.1007/s11771-015-2980-1

Rhoades JD, Manteghi NA, Shouse PJ, Alves WJ (1989) Soil electrical conductivity and soil salinity: new formulations and calibrations. Soil Sci Soc Am J 53:433–439. https://doi.org/10.2136/sssaj1989.03615995005300020020x

Rinaldi Victor A, Cuestas German A (2002) Ohmic conductivity of a compacted silty clay. Journal of Geotechnical and Geoenvironmental Engineering 128:824–835. https://doi.org/10.1061/(ASCE)1090-0241(2002)128:10(824)

Ronald AE, Ronald CG (1982) Electrical resistivity used to measure liquefaction of sand. Journal of Geotechnical Engineering 108:779–783

Ruedrich J, Bartelsen T, Dohrmann R, Siegesmund S (2011) Moisture expansion as a deterioration factor for sandstone used in buildings. Environmental Earth Sciences 63:1545–1564. https://doi.org/10.1007/s12665-010-0767-0

Samouëlian A, Cousin I, Tabbagh A, Bruand A, Richard G (2005) Electrical resistivity survey in soil science: a review. Soil and Tillage Research 83:173–193. https://doi.org/10.1016/j.still.2004.10.004

Sendrós A, Himi M, Lovera R, Rivero L, Garcia Artigas R, Urruela A, Casas A (2020) Electrical resistivity tomography monitoring of two managed aquifer recharge ponds in the alluvial aquifer of the Llobregat River (Barcelona, Spain). Near Surf Geophys.https://doi.org/10.1002/nsg.12113

Shah PH, Singh DN (2004) A simple methodology for determining electrical conductivity of soils. J ASTM Int 1:1–11. https://doi.org/10.1520/JAI12128

Shan W, Liu Y, Hu ZG, Xiao JT (2015) A model for the electrical resistivity of frozen soils and an experimental verification of the model. Cold Reg Sci Technol 119:75–83. https://doi.org/10.1016/j.coldregions.2015.07.010

Shevnin V, Mousatov A, Ryjov A, Delgado-Rodriquez O (2007) Estimation of clay content in soil based on resistivity modelling and laboratory measurements. Geophys Prospect 55:265–275. https://doi.org/10.1111/j.1365-2478.2007.00599.x

Snapp M, Tucker Kulesza S, Koehn W (2017) Electrical resisitivity of mechancially stablized earth wall backfill. J Appl Geophys 141:98–106. https://doi.org/10.1016/j.jappgeo.2017.04.011

Soga K, Mitchell J (2005) Fundamentals of soil behavior, 3rd Edition, vol 3. Wiley & Sons, New York, USA

Tabbagh J, Samouëlian A, Tabbagh A, Cousin I (2007) Numerical modelling of direct current electrical resistivity for the characterisation of cracks in soils. J Appl Geophys 62:313–323. https://doi.org/10.1016/j.jappgeo.2007.01.004

Tang LY, Wang K, Jin L, Yang GS, Jia HL, Taoum A (2018) A resistivity model for testing unfrozen water content of frozen soil. Cold Reg Sci Technol 153:55–63. https://doi.org/10.1016/j.coldregions.2018.05.003

Wang J, Huang S, Guo W, Qiu Z, Kang K (2020) Experimental study on fracture toughness of a compacted clay using semi-circular bend specimen. Eng Fract Mech 224:106814. https://doi.org/10.1016/j.engfracmech.2019.106814

Wang J, Liu W, Chen WW, Liu P, Jia BB, Xu H, Wen L (2019) Study on the mechanism of loess landslide induced by chlorine salt in Heifangtai terran. Japanese Geotechnical Society Special Publication 7:159–167. https://doi.org/10.3208/jgssp.v07.024

Wang JJ, Hayakawa KL (1993) Maximum slope method for evaluating thermal conductivity probe data. J Food Sci 58:1340–1345. https://doi.org/10.1111/j.1365-2621.1993.tb06179.x

Waxman MH, Smits LJM (1968) Electrical conductivities in oil-bearing shaly sands. Soc Petrol Eng J 8:107–122. https://doi.org/10.2118/1863-A

Weisbrod N, Dragila MI (2006) Potential impact of convective fracture venting on salt-crust buildup and ground-water salinization in arid environments. J Arid Environ 65:386–399. https://doi.org/10.1016/j.jaridenv.2005.07.011

Xu P, Qian H, Zhang Q, Zheng L (2021a) Exploring the saturated permeability of remolded loess under inorganic salt solution seepage. Eng Geol 294:106354. https://doi.org/10.1016/j.enggeo.2021.106354

Xu P, Zhang Q, Qian H, Li M, Yang F (2021b) An investigation into the relationship between saturated permeability and microstructure of remolded loess: a case study from Chinese Loess Plateau. Geoderma 382:114774. https://doi.org/10.1016/j.geoderma.2020.114774

Xue S, Sun Q, Jia H, Zhang L, Wang S (2021) Effects of water content and salinity on the porosity structure and resistivity of loess soil sintered at 1000 °C. Arab J Geosci 14:1446. https://doi.org/10.1007/s12517-021-07883-w

Yan X, Duan Z, Sun Q (2021) Influences of water and salt contents on the thermal conductivity of loess. Environmental Earth Sciences 80:52. https://doi.org/10.1007/s12665-020-09335-2

Yang YL, Zhang T, Liu SY (2020) Influence factor analysis and calculation model for thermal/electrical resistivity of geomaterials. Measurement 152:107373. https://doi.org/10.1016/j.measurement.2019.107373

Yin X, Liu Q, Pan Y, Huang X, Wu J, Wang X (2021) Strength of stacking technique of ensemble learning in rockburst prediction with imbalanced data: comparison of eight single and ensemble models. Nat Resour Res 30:1795–1815. https://doi.org/10.1007/s11053-020-09787-0

You Z, Lai Y, Zeng H, Yang Y (2020) Influence of water and sodium chloride content on corrosion behavior of cast iron in silty clay. Constr Build Mater 238:117762. https://doi.org/10.1016/j.conbuildmat.2019.117762

Yun TS, Jeong YJ, Han TS, Youm KS (2013) Evaluation of thermal conductivity for thermally insulated concretes. Energy and Buildings 61:125–132. https://doi.org/10.1016/j.enbuild.2013.01.043

Zha F, Liu S, Du Y, Cui K, Xu L (2010) Characterization of compacted loess by electrical resistivity method. Paper presented at the Geo-Shanghai International Conference 2010, Shanghai, China,

Zhang DW, Cao ZG, Fan LB, Liu SY, Liu WZ (2014) Evaluation of the influence of salt concentration on cement stabilized clay by electrical resistivity measurement method. Eng Geol 170:80–88. https://doi.org/10.1016/j.enggeo.2013.12.010

Zhang T, Liu SY, Cai GJ (2018) Correlations between electrical resistivity and basic engineering property parameters for marine clays in Jiangsu. China Journal of Applied Geophysics 159:640–648. https://doi.org/10.1016/j.jappgeo.2018.10.012

Zhao KY, Xu Q, Liu FZ, Xiu DH, Ren XH (2020) Field monitoring of preferential infiltration in loess using time-lapse electrical resistivity tomography. J Hydrol 591:125278. https://doi.org/10.1016/j.jhydrol.2020.125278

Geomaterial segmentation method using multi-dimensional frequency analysis based on electrical resistivity tomography. Eng Geol 105925. https://doi.org/10.1016/j.enggeo.2020.105925

Zhou M, Wang J, Cai L, Fan Y, Zheng Z (2015) Laboratory investigations on factors affecting soil electrical resistivity and the measurement. IEEE Trans Ind Appl 51:5358–5365. https://doi.org/10.1109/TIA.2015.2465931

Zhou WF, Beck B, Adams A (2002) Effective electrode array in mapping karst hazards in electrical resistivity tomography. Environ Geol 42:922–928. https://doi.org/10.1007/s00254-002-0594-z